GE Oil & Gas

Francesco Balduzzi, Dept. of Industrial Engineering, University of Florence
Giovanni Ferrara, Dept. of Industrial Engineering, University of Florence
Alberto Babbini, GE Oil & Gas
Riccardo Maleci, GE Oil & Gas

DOWNSTREAM TECHNOLOGY SOLUTIONS | PRODUCTS & SERVICES

Reciprocating compressor cylinder's cooling: a numerical approach using computational fluid dynamics with conjugate heat transfer

Abstract

The large reciprocating compressor segment is increasing its attention on efficiency improvements. The working cycle of a reciprocating compressor generates heat, mainly due to compression transformation and friction phenomena. This excess heat translates to lower volumetric efficiency and higher gas discharge temperatures. Regulations such as the American Petroleum Institute's API 618 guidelines for reciprocating compressors require a cylinder cooling system. This means that an effective cooling circuit design is essential in achieving a good balance between refrigerating potential and system capacity.

It is important to apply a systematic methodology when evaluating the heat transfer process. Additionally, because the experimental characterization of the circuit is complex and case-dependent, the use of a numerical approach should result in the most favorable and generalizable outcome. Of the available techniques, 3-D analysis shows great potential, although several phenomena must be accounted for to accurately model the system.

GE Oil & Gas, in conjunction with the University of Florence, performed a conjugate heat transfer (CHT) analysis of a double-acting water-cooled reciprocating compressor cylinder. The 3-D flow field of the water circuit and the thermal conduction inside the solid metal are solved simultaneously. GE also provides the best practices for defining consistent boundary conditions for the metal body, with special attention given to the heat transfer coefficient (HTC) values for the suction and discharge gas chambers, the compression chamber, and the external ambient conditions. The assessment of the numerical methodology is completed with an investigation on the influence of wall roughness and buoyancy effects.

Nomenclature

B	Bore	[m]
Bo	Buoyancy number	[-]
CHT	Conjugate Heat Transfer	
c_p	Specific heat	[J/(kg K)]
D	Diameter	[m]
g	Acceleration of gravity	[m/s^2]
Gr	Grashof-number	[-]
h	Roughness height	[m]
h^+	Dimensionless roughness	[-]
h^+_s	Equivalent sand-grain roughness	[-]
H	Enthalpy	[J/kg]
HTC	Heat Transfer Coefficient	[W/(m^{2}K)]
k	Turbulent kinetic energy	[m^2/s^2]
l	Reference length	[m]
Nu	Nusselt-number	[-]
Pr	Prandtl-number	[-]
q	Heat flux	[W/m^2]
Ra	Rayleigh-number	[-]
R_A	Average roughness height	[m]
Re	Reynolds number	[-]
T	Temperature	[K]
U_p	Mean piston speed	[m/s]
U_τ	Friction velocity	[m/s]
V	Instantaneous volume	[m^3]
V_d	Cylinder displacement	[m^3]
y^+	Dimensionless wall distance	[-]
y_{SL}	Height of the viscous sublayer	[m]
β	Volumetric thermal expansion coefficient	[K^{-1}]
λ	Thermal conductivity	[W/(m K)]
μ	Dynamic viscosity	[Pa s]
ν	Kinematic viscosity	[m^2/s]
ρ	Density	[kg/m^3]
ω	Specific dissipation rate of k	[s^{-1}]

Introduction

The four main categories of energy losses in reciprocating compressors are: mechanical friction losses, electrical losses, cycle losses (compression and expansion) and thermodynamic losses, as analyzed in-depth by Possamai and Todescat [1].

For thermodynamic losses, the most critical issues are related to both pressure losses along gas circuits (suction and discharge) and the heat loss from the working fluid through solid metal walls. The cooling system's function is to keep thermal dilatation under control and to protect the mechanical components from overheating caused by unit malfunction. In addition, cooling systems improve heat distribution on the whole cylinder assembly, avoiding hot spots that endanger mechanical integrity and cold spots that can lead to fluid condensation.

Early water jacket designs applied the thermosyphonic approach using big volumes of coolant and low capacity of the cooling circuit. While some recently introduced forced-liquid coolant systems follow API 618 guidelines, the general design trends still involve cooling jackets that are oriented to the previous, conservative approach.

As the market shifted its focus to power saving opportunities, equipment manufacturers have started paying more attention to improving fluid-dynamic efficiency by reducing the cooling jacket volume to make more room for gas chambers. Volume reduction cannot be effectively undertaken without a thorough analysis of the cooling jacket inside the cylinder to avoid a reduction in heat removal capability from critical surfaces.

A proper fluid dynamic design of the whole machine should aim to guarantee, on the one hand, a gas duct shape that results in minimal pressure loss of the working fluid and, on the other hand, effective system cooling. In particular, the essential requirement is the assessment of the proper sizing of the cooling circuit to reduce its occupancy volume to avoid unnecessary gas duct shape restrictions and improve performance.

Many past studies have focused on heat transfer in reciprocating compressors. Most of these studies concentrated on simplified approaches, such as the one proposed by Ooi [2], in which the whole system of compressor components is represented through a network of analytical elements.

Higher level studies on full 3-D simulations were performed by Aigner [3] and Disconzi [4], but their simulations only involve heat transfer for working gas without accounting for thermal conduction inside the solid metal. The metal structure is considered in Abidin's work [5], but attention is still focused on the behavior of working gas because no cooling circuit is present due to the very small size of the analyzed machine. Moreover, fluid and metal domain are solved separately and their results are iteratively coupled.

Simulation Approach

This activity aims to define a numerical approach for the simulation of heat transfer in a double-acting water-cooled reciprocating compressor cylinder. The simultaneous solution of the water-circuit flow field and the thermal conduction inside the solid metal (conjugate heat transfer) can be obtained by performing a steady-state analysis, considering a constant mass flow rate through the cooling circuit.

A more accurate investigation also requires the simultaneous simulation of the flow of the working fluid (such as gas) that is responsible for heat generation. In this case, however, the steady-state approach is not applicable because the increase in gas temperature occurring inside the compression chamber can be obtained only with the execution of a transient simulation of the working cycle [5]. The complexity of the 3-D domain and the grid requirements would lead to an excessively large calculation time, making the steady-state analysis the most favorable approach.

Therefore, heat transfer with the gas is modeled as a boundary condition to be applied on the solid walls of the metal body, whose half section is shown in Figure 1, together with the water body.

In light of the above considerations, several phenomena should be considered:

- Forced convection inside suction and discharge gas ducts
- Natural convection on the external surface
- Forced convection and heat generated by friction inside the compression chamber

In the matter of heat transfer related to friction between piston and liner, the heat flux (q) through the boundary surfaces is known from experimental data.

Regarding heat transfer related to a generic convective process, the metal temperature is calculated by evaluating the heat flux through the boundary surfaces, as defined by Equation 1:

$$q = HTC \cdot (T_W - T_{bulk}) \quad (1)$$

where T_w is the unknown metal temperature at the wall surface, *HTC* is the convective heat transfer coefficient between fluid and metal, and T_{bulk} is the undisturbed fluid temperature.

The CHT simulation requires the imposition of the quantities

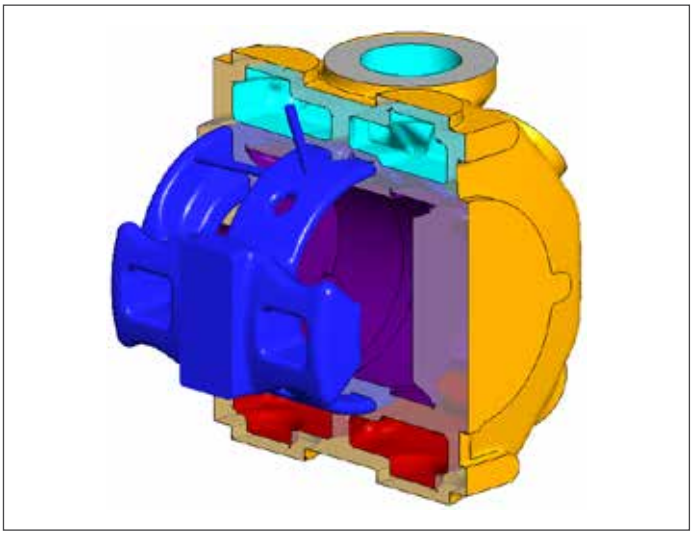

Figure 1 – Domain for the CHT analysis: water body in blue and surfaces of the metal body in orange (external), violet (compression chamber), red (discharge ducts) and light blue (suction ducts)

HTC and T_{bulk} as inputs, although they are not known a priori. Therefore, a proper model of all the convection processes needs to be assessed to accurately define the boundary conditions.

The most trivial approach makes use of empirical correlations available in literature, largely assessed and validated with experimental data dealing with simple geometry. This method

requires a high level of simplification since the actual geometry of the compressor needs to be approximated by considering appropriate analogies with the literature examples.

For external natural convection, McAdams [6] provides a standard example of Nusselt-number (*Nu*) correlations for both vertical plates (Equation 2), recommended for a Grashof-number (*Gr*) greater than 10^9, and horizontal plates, hot upper surface (Equation 3) and hot lower surface (Equation 4), recommended over a Rayleigh-number range of $10^7 < Ra < 10^{10}$:

$$Nu = 0.13 \cdot (Gr \cdot Pr)^{1/3} \quad (2)$$

$$Nu = 0.15 \cdot Ra^{1/3} \quad (3)$$

$$Nu = 0.27 \cdot Ra^{1/4} \quad (4)$$

where the dimensionless numbers are defined by the following equations:

$$Nu = \frac{HTC \cdot l}{\lambda} \quad (5)$$

$$Gr = \frac{g\beta \cdot (T_W - T_{bulk}) \cdot l^3}{\nu^2} \quad (6)$$

$$Pr = \frac{c_p \mu}{\lambda} \quad (7)$$

$$Ra = Gr \cdot Pr \quad (8)$$

Concerning the condition of forced convection inside the ducts, several correlations exist for turbulent incompressible flows through circular tubes. From the simplest relationship proposed by Dittus-Boelter [7] to the more complex equations of Petukhov-Popov [8] or Sleicher-Rouse [9], correlations are provided in the form $Nu = f(Re,Pr)$ valid for long tubes (L/D > 60) and within a Reynolds number range of about $10^4 < Re < 10^6$.

To increase the complexity of the representation, Bhatti and Shah [10] developed a correction to estimate the effect of the shape of the entrance region:

$$Nu = Nu_{fd} \cdot \left(1 + \frac{c}{(L/D)^n}\right) \quad (9)$$

where *c* and *n* are empirical constants, depending on the entrance configuration (elbow, round bend, and so on) and Nu_{fd} is the Nusselt-number in fully developed conditions.

Finally, various correlations for the convection inside the compression chamber have been presented in the past, both in the field of reciprocating compressors and reciprocating internal combustion engines. Following the advice of Fagotti [11], which evaluated the capability of different correlations in fitting the experimental data for a small hermetic reciprocating compressor, best results are provided by the Annand formulation [12], expressed as a function of the average piston speed (U_p) and the piston bore (B) as shown in Equation 10:

$$Nu = A \cdot \left(\frac{\rho U_p B}{\mu}\right)^b \quad (10)$$

The use of literature correlations as a boundary condition for the external natural convection can be considered suitable because the amount of heat transfer with the ambient environment represents only a small amount of the total heat exchange, as will be described later. For that reason, an inaccuracy in the estimation of the *HTC* value is deemed to not significantly affect the overall accuracy of the calculation.

On the contrary, in case of internal forced convection inside suction and discharge gas ducts, the approximation introduced by such an approach is excessively large, as will be discussed later. Therefore, a specific 3-D CFD simulation is required for both the suction and discharge ducts to provide the actual local distribution of *HTC* and T_{bulk} values. As an example, Figure 2 shows the HTC contour plot for the suction geometry resulting from a steady-state simulation of the gas flow.

The *HTC* values are presented in a dimensionless form, such as those noted as a function of a reference value computed by adopting the literature correlations for the suction duct ($HTC^* \equiv HTC/HTC_{ref}$). Due to the flow conditions inside the ducts, the steady-state assumption is a reasonable approximation because the thermo-dynamic state of the gas does not experience a significant change while flowing through the pipeline. This *HTC* field, as well as the one for the discharge duct obtained in an analogous manner, must be patched as a boundary condition for the CHT simulation.

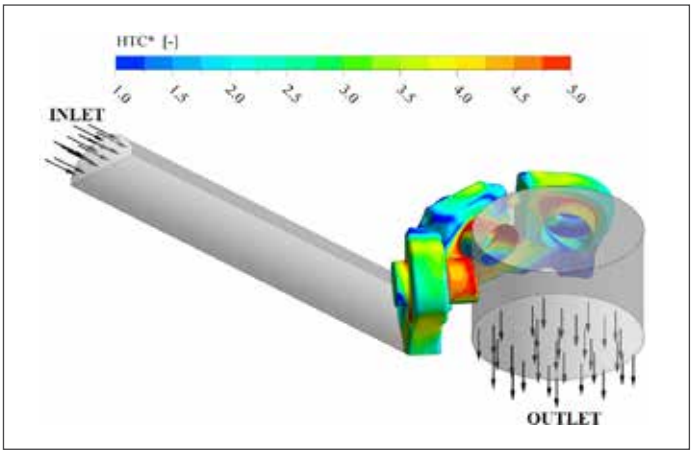

Figure 2 – HTC distribution on the suction duct walls

Finally, the use of Annand's correlation to determine *HTC* for the compression chamber can be considered a valid alternative to avoid a transient CFD simulation of the operating cycle. Nevertheless, because the gas properties (ρ, *T*, μ, etc.) are notably variable inside the cylinder during a complete revolution, a 0-D modeling of the compression cycle (Figure 3) is required to obtain a representative trend of in-cylinder *HTC* and temperature as a function of the instantaneous displacement (Figure 4). Temperature values are reported in a dimensionless form, such as those noted as a function of the gas discharge temperature ($T^* \equiv T/T_d$).

An average effective value of both *HTC* and T^* was computed from the time-dependent functions to be adopted for the steady-state simulations.

The proposed approach is summarized in Figure 5, which indicates all boundary conditions used to simulate conjugate heat transfer between the solid cylinder body and the fluid cooling circuit.

Note that both the gas ducts CFD model and the cylinder 0-D model require the knowledge of the metal wall temperature T_w as a boundary condition to determine the convection process. Because these data must be obtained from the CHT analysis, it is necessary to use an iterative routine that updates the boundary conditions and repeats the entire set of simulations.

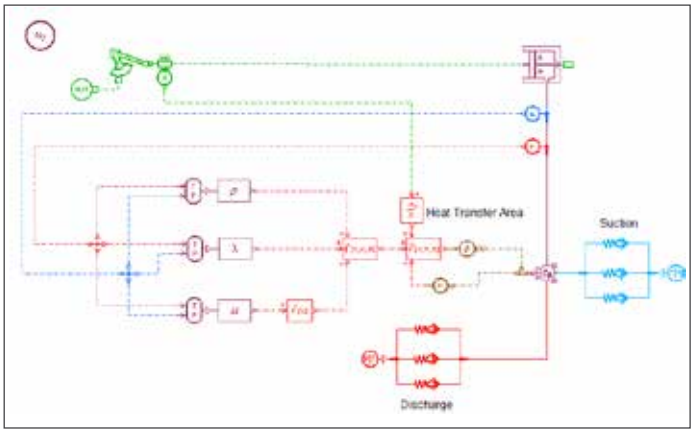

Figure 3 – Scheme of the 0-D model for the simulation of the working cycle

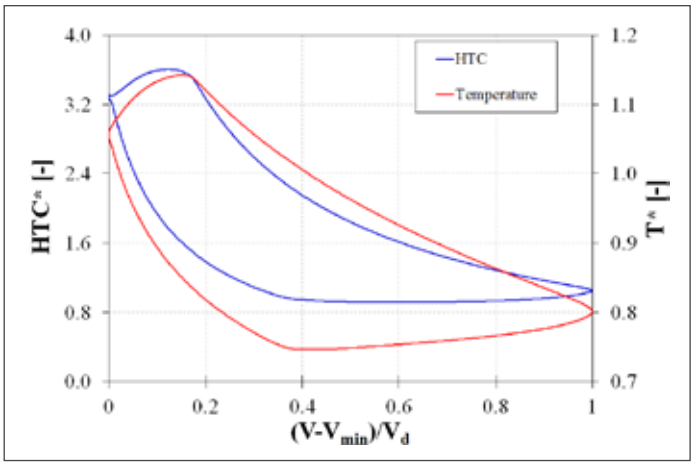

Figure 4 – Outputs of the 0-D model: trends of HTC and temperature as a function of the instantaneous displacement

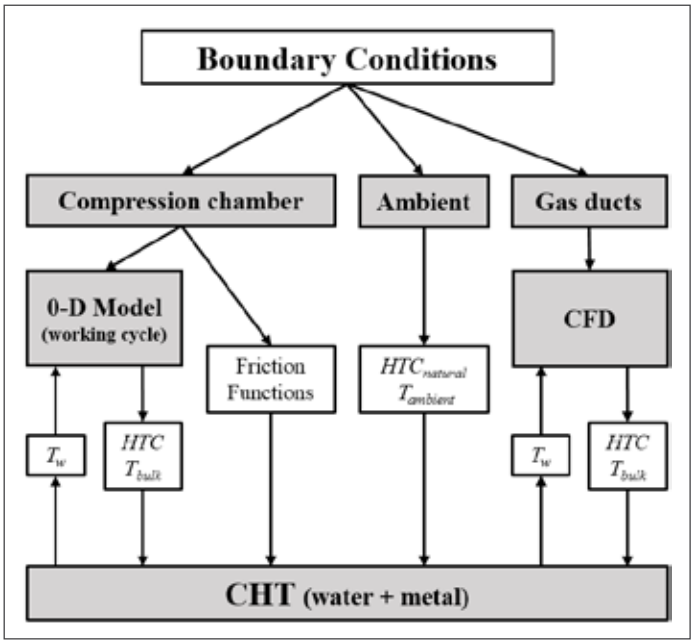

Figure 5 – Simulation approach: conceptual scheme for determining the boundary conditions

Roughness and Buoyancy

The presence of wall roughness affects turbulence production near the wall, increasing both wall shear stress and wall heat transfer. As reported by Webb [13], Nikuradse developed a friction correlation to analyze this phenomenon for flow over "sand-grain" roughness. This report shows that the modification in the law of the wall is due to the dimensionless roughness height h^+ of the sand-grain elements:

$$h^+ = h \cdot U_\tau / \nu \tag{11}$$

The logarithmic law for the dimensionless temperature for smooth walls (T^+_{smooth}) is then modified by introducing a coefficient ΔB, function of h^+, as shown in Equation 12 [14]:

$$T^+ = T^+_{smooth} - \Delta B(h^+) \tag{12}$$

Under these conditions, three roughness regimes can be defined, showing that the weight of the surface finishing cannot be evaluated independently from the flow conditions:

- Hydraulically smooth wall: $0 \le h^+ \le 5$
- Transitional roughness regime: $5 \le h^+ \le 70$
- Fully rough flow: $h^+ \le 70$

In the case of generic roughness, the above equations can be applied after defining an "equivalent" sand-grain roughness (h^+_s) – in other words, an equivalent layer of closely packed spheres having an average roughness height of h_s. Burck [15] concluded that the heat-transfer data of all roughness types yield the same performance if evaluated at equal h^+_s values. The main issue is related to the conversion of measured surface roughness parameters to h^+_s values. While different correlations exist in literature, the one selected here was provided by Adams [16], who computed the value of R_A for a single row of spheres of diameter h_s, leading to the following relationship:

$$h_s = 11.03 \cdot R_A \tag{13}$$

In addition, the effect of roughness is weakened if considered in combination with a buoyancy-driven flow. Various experiments were conducted by Symolon [17] for both rough and smooth heated tubes in a mixed convection regime (transition between natural and forced convection) with a Reynolds number range of about $2600 < Re < 70000$. The results demonstrated that the effect of roughness decreases with the buoyancy number (Bo), and the condition for the onset of mixed convection is $Bo > 10^{-6}$, where:

$$Bo = \frac{Gr}{Re^3 Pr^{1/2}} \tag{14}$$

gives a qualitative indication of the influence of buoyancy on forced convection.

Numerical Setup

All simulations focus on the analysis of a double-acting cast iron cylinder with a bore of 770 mm, which compresses pure nitrogen. The investigated geometries for the CHT analysis include all solid components of the cylinder and water circuit. The domain is oriented so that the water enters from an inlet pipe located on the bottom of the cylinder, which is the side where the pressurized hot gas is discharged. The main characteristics of the studied compressor are summarized in Table 1.

Parameter	Units	Value
Bore	[mm]	770
# Suction Valves	[-]	3 + 3
# Discharge Valves	[-]	3 + 3
Suction Temperature (T^*)	[-]	77.95%
Suction Pressure	[Pa]	1200000
Discharge Pressure	[Pa]	2700000

Table 1 – Compressor specifications

CHT Model

Simulations were performed with the ANSYS CFX software package using a 3-D steady-state Reynolds-Averaged Navier-Stokes (RANS) analysis. With this approach, all conservation equations are solved for the water fluid region. For the solid region, only the equation for heat transfer is solved, but with no flow, resulting in the following formulation for the enthalpy h in the case of static solid region [14]:

$$\frac{\partial(\rho H)}{\partial t} = \nabla \cdot (\lambda \nabla T) + S_E \qquad (15)$$

which can account for heat transport due to conduction and volumetric heat sources (S_E).

The buoyancy model was activated for the water region, because free convection plays a relevant role in terms of low mass flow rates (i.e., low fluid velocities), large fluid volumes, and appreciable temperature differences. Therefore, the requirement in terms of near wall refinement for the spatial discretization of the domain is very strict: y^+ values lower than one are necessary to properly resolve the thermal boundary layer.

The standard k-ω turbulence model was adopted for the water domain due to its ability to better describe the boundary layer than the ε-based models. This model was shown to be able to integrate through the viscous sublayer [18], in agreement with the y^+ requirements. The automatic near-wall treatment was used. This treatment automatically switches from wall-functions to a low-Re approach as the mesh is refined, allowing a consistent y^+ mesh refinement from coarse to fine grids.

Because the surface finishing of the water chamber is non-smooth (non-negligible average roughness height R_A), a specific simulation was carried out by applying an equivalent sand grain roughness for the walls to assess the roughness regime for our case study. The Adams [16] correlation was used for the definition of the h_s parameter.

Velocity-inlet and pressure-outlet boundary conditions were supplied for the simulation of the water flow (Figure 6), and all the solid boundaries were defined as "fluid-solid interfaces" where the conservation of the heat flux is guaranteed with the metal body. The water inlet temperature (T^*) was set to 80.4 percent of the gas discharge temperature.

With one exception, the boundary conditions for the solid region were all defined as thermal boundary conditions with the *HTC* and T_{bulk} distributions applied. For the walls in contact with the moving piston and rod, an additional heat source was imposed to account for friction heating.

The mesh discretization for the water body (Figure 6) was achieved by a tetrahedral unstructured grid in the core region of the fluid volume. To accurately describe the development of the thermal boundary layer, an extrusion of 16 prism layers was placed adjacent to the viscous wall, with an expansion ratio of adjacent cells below 1.1 to avoid excessively large elements far from the wall. To guarantee the requirement of y^+~1, the height of the first element at the wall was diversified for each surface depending on the flow velocity. The size of the tetrahedral elements in the core region was kept constant to ensure an accurate description of buoyancy-driven flows. As a result, a total number of $1.3*10^7$ elements was obtained.

The metal body was entirely discretized by using tetrahedral elements (Figure 7). Having fewer requirements for solving the RANS equations in a solid region allowed the definition of a coarser mesh, with a size of $1.4*10^6$ elements.

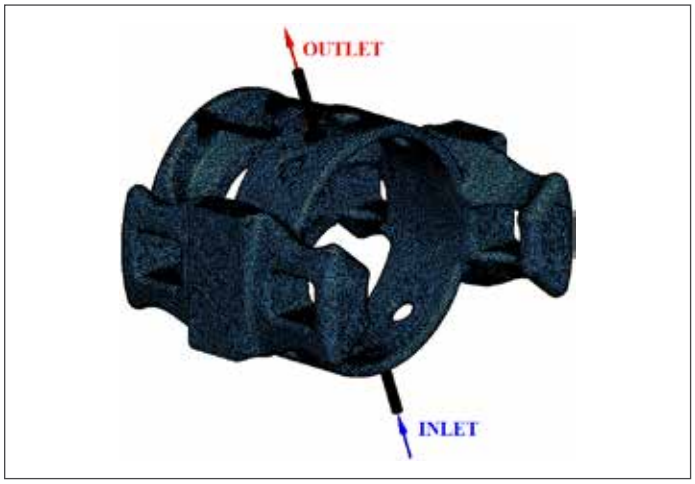

Figure 6 – Computational grid for the water body (surface mesh)

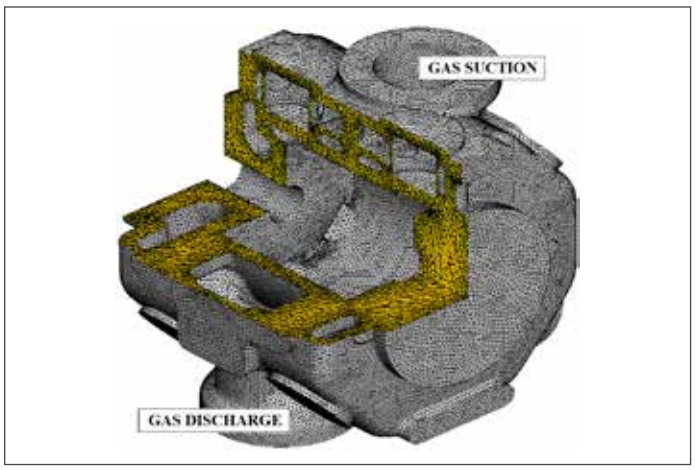

Figure 7 – Computational grid for the metal body (surface mesh and section view of the body mesh)

Gas Ducts Model

The numerical settings and mesh properties for the steady-state 3-D CFD simulations of the working gas inside the suction and discharge gas ducts, modeled as an ideal compressible gas with constant viscosity, are not discussed here because they are out of scope.

Moreover, their assessment and validation has been presented by various authors in recent works (see References [19], [20] and [21]), where details for the sensitivity analysis on the simulation parameters can be found.

Results

To assess the most appropriate simulation settings, the numerical results of CHT simulations were analyzed. As previously noted, an iterative practice was used to help ensure reliable results.

The first step was the computation of the initial estimate values of the *HTC* for the gas ducts to be adopted for the first iteration of the CHT simulation. In particular, the HTC_{corr} value was obtained using the Petukhov-Popov correlation [8], along with the correction proposed by Bhatti and Shah [10] for a 90° elbow.

The computed temperature distributions on the gas chamber walls then were imposed as boundary conditions for the CFD simulations of both the suction and discharge gas ducts. As a result, more realistic *HTC* and T_{bulk} distributions were calculated and used for the second iteration of the CHT simulation.

The *HTC* values derived from the literature correlations for both the suction and discharge ducts were found to be considerably lower than the ones resulting from the CFD analysis, being roughly equal to only 20 percent of the maximum local value. This iterative method was repeated until convergence was reached.

Additionally, the influence of wall roughness was evaluated, as well as the relevance of buoyancy phenomena.

Influence of Gas Ducts HTC

The need for executing the iteration between CHT and CFD simulation was investigated by analyzing the difference between the results obtained with the simple literature correlation and those obtained after the dedicated CFD gas ducts simulation.

Figure 8 highlights the modification in terms of dimensionless temperature (*T**) of the metal for the two iterations of the CHT model for the suction duct wall.

The computed temperatures in the second iteration were substantially lower, especially in the region of the automatic valves. In both cases the temperature at the gas inlet leveled off at the same value of the gas itself, while moving toward the hot part of the cylinder. The temperature increase was almost halved with the second iteration.

This behavior is due to an increase in the heat exchange between gas and metal, as demonstrated in Figure 2. The CFD suction duct simulation revealed that the actual *HTC* is almost twice that of the HTC_{corr} on average, with peak values more than five times greater.

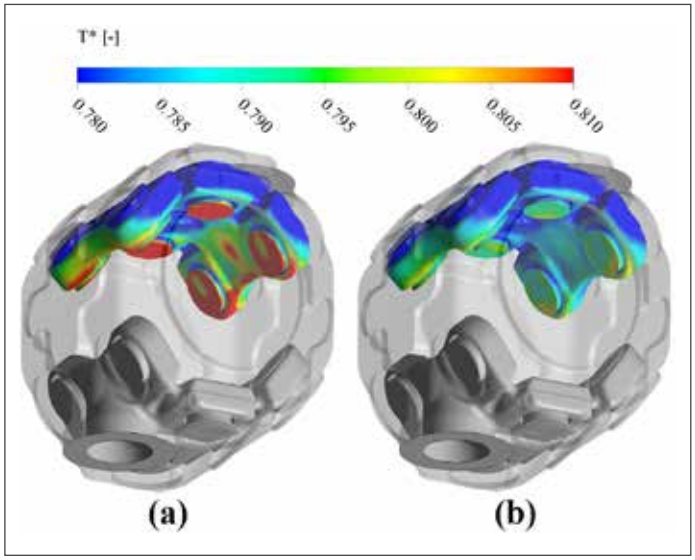

Figure 8 – Temperature field on the suction duct wall of the metal body: (a) Iteration 1, (b) Iteration 2

The response in terms of total heat transfer of the entire surfaces was quantified, as reported in Table 2. Even if the greatest variation in the heat transfer was observed for the suction duct, which has a cooling effect on the machine, the global heating of the water was found to be greater (+31.7 percent). This was determined by the higher magnitude of the heat provided by the discharge gas, due to its high temperature.

A third iteration was deemed unnecessary since it would lead to a further negligible variation, being lower than 3 percent for the water ΔT.

VARIABLE	VARIATION
Heat Transfer Suction Duct [W]	+105.8%
Heat Transfer Discharge Duct [W]	+57.4%
ΔT° Water [K]	+31.7%

Table 2 – Variation of thermal response of the CHT results: Iteration 2 vs. Iteration 1

Roughness and Buoyancy

To evaluate the influence of both the wall roughness and the natural convection, dimensionless parameters were used, as defined earlier.

The results were more easily clarified through the identification of five different regions in the simulated domain – each corresponding to different features (see Figure 9):

- Regions 1-2: horizontal chambers for thermal isolation of the cold side of the compressor from the hot side, characterized by large sections and low fluid velocity
- Region 3: annular chamber for rod package cooling, characterized by large sections and low fluid velocity
- Regions 4-5: cylinder water jacket (cold and hot side), characterized by small sections and high fluid velocity

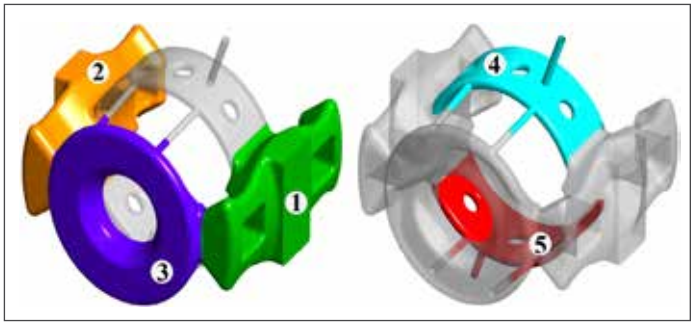

Figure 9 – Conceptual subdivision of the fluid domain

Figure 10 shows the results in terms of equivalent sand-grain roughness h^+_s distribution. The greatest portion of the domain is in the hydraulically smooth regime ($h^+_s < 5$), and only some surfaces are in the transitional regimes. In particular, higher h^+_s values correspond with regions characterized by higher flow velocity due to the lower thickness of the water jacket (regions 4 and 5). In any case, the condition is always far from the fully rough regime ($h^+_s > 70$).

To be classified as rough, the surface roughness parameter h_s has to be greater than the scale of the viscous layer (maximum height of y^+~11), as indicated by Schumann [22].

Therefore, the height of the viscous sub-layer (y_{SL}), proportional to ν/U^*, was computed and depicted in Figure 11. Again, roughness is negligible in all the regions with low speed

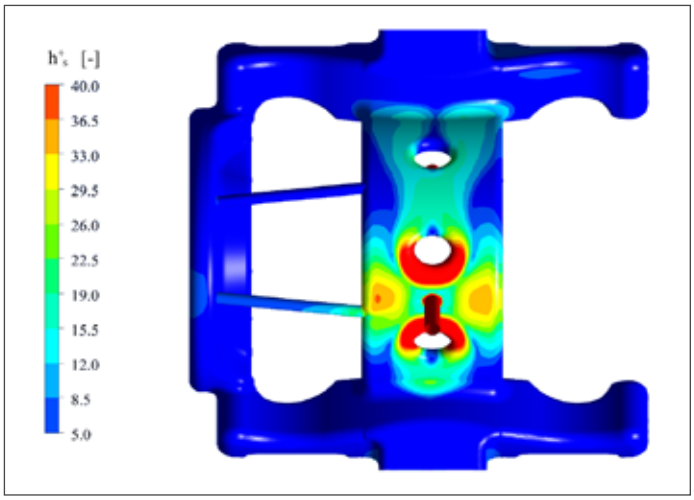

Figure 10 – Equivalent sand-grain roughness h^+_s on the solid walls of the water body

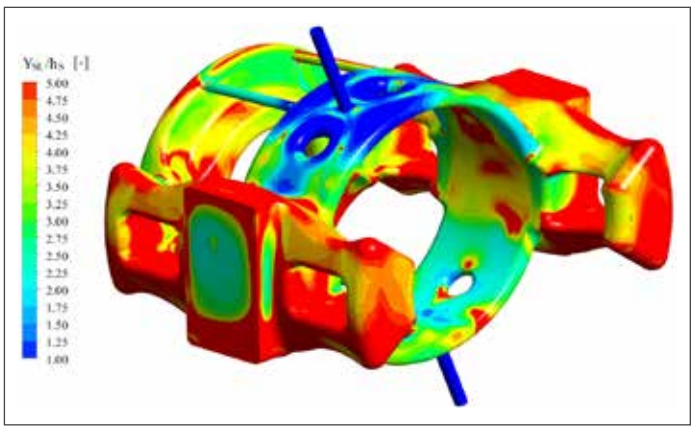

Figure 11 – Height of the viscous sublayer on the solid walls of the water body

(regions 1, 2 and 3) because the viscous layer height is three to five times the value of h_s. For the water jacket, the height of the viscous layer is of the same order of magnitude of h_s, confirming the presence of a transitional regime.

Finally, to quantify the entity of free convection for the studied geometry, the values of Gr, Re and Bo were computed for all the aforementioned regions, as presented in Table 3.

The natural convection prevails by far in almost 88 percent of the volume of the cooling circuit with the buoyancy number being three orders of magnitude greater than the limit suggested by Symolon [17]. Forced convection is identified only in the faster regions (i.e. 4 and 5) where the Bo values indicate mixed convection. These flow conditions confirm the necessity of a fine discretization of both the near wall region and the fluid core.

Region	Gr	Re	Bo	Volume/Total Volume
1	$5.4*10^8$	$4.5*10^3$	$2.4*10^{-3}$	32%
2	$5.7*10^8$	$3.4*10^3$	$5.9*10^{-3}$	32%
3	$5.1*10^7$	$1.3*10^3$	$8.6*10^{-3}$	24%
4	$1.5*10^7$	$7.7*10^3$	$1.3*10^{-5}$	6%
5	$1.4*10^7$	$4.4*10^3$	$6.6*10^{-5}$	6%

Table 3 – Buoyancy properties of each region of the fluid domain

Heat Transfer Distribution

Preliminary considerations were very important in assessing an effective simulation of the fluid-solid conjugate heat transfer that ultimately would provide valid results.

The last step of the investigation was dedicated to a detailed examination of the cooling performance of the specific geometry. In particular, attention was focused on determining the regions characterized by higher/lower heat transfer. To this end, the heat flux (q) on the water-metal interface is shown in Figure 12 in a dimensionless form (q^*) as a function of the average value ($q^* \equiv q/q_{ave}$).

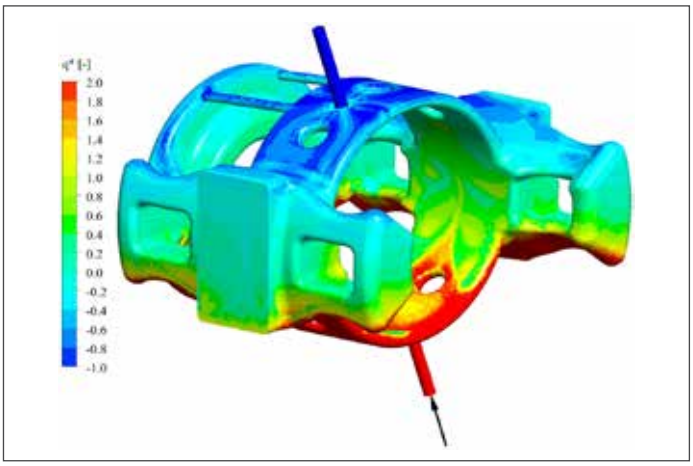

Figure 12 – Heat flux contours on the water-metal interface

As expected, the hot side of the cylinder water jacket (Region 5) was found to be responsible for the highest values of the heat flux. The temperature difference between the hot discharge gas and the cold entering water was about 19.6 percent. Conversely, on the cold side of the cylinder water jacket, the heat flux is negative; the situation is reversed since the water is warming the cylinder. In fact, the water circuit is designed

to work as a thermostating element to guarantee more metal body temperature uniformity, reducing deformations related to thermal dilatation.

The absolute value of the heat transfer then was quantified for the five regions of Figure 9, as reported in Table 4. Region 5 is the main area responsible for the overall heat exchange. Despite the fact that it represents only 6 percent of the water volume, it plays the leading role due to the coupled effect of forced convection and high metal surface temperature. In contrast, the cooling effect of the water on the cold side is weak, as well as the mean contribution of the annular chamber.

REGION	HEAT TRANSFER [%]
1	18.6%
2	16.5%
3	9.7%
4	-7.2%
5	62.3%

Table 4 – Contribution of the fluid regions to the overall heat absorbed by water

The volume rendering of the water temperature field shown in Figure 13 indicates that the temperature increase of the water flowing inside the annular chamber is 50 percent higher than the increase at the water outlet. This can be explained by the presence of a stagnation region inside the chamber that does not permit an efficient use of all of the volume available to the cooling system.

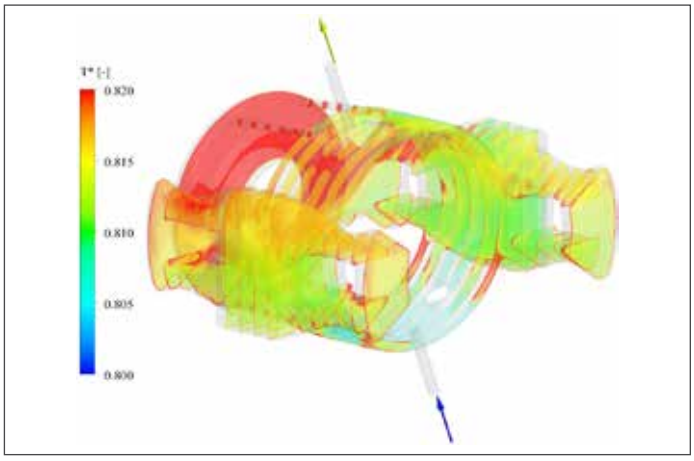

Figure 13 – Volume rendering of the water temperature field

Finally, Figure 14 shows the temperature distribution for the solid domain. The temperature range is obviously wider in this case, varying from gas suction to discharge temperatures. However, very high temperatures are found only in a small portion of the metal body located on the bottom of the cylinder. Most of the metal surrounding the compression chamber is at a temperature closer to the suction temperature, indicating good isolating capability of the water body.

Table 5 reports the contribution of each metal surface to the global heat transfer capability with the values scaled by the heat absorbed by water. It is evident that forced convection inside the gas ducts plays the more relevant role, while the phenomena occurring in the gas chamber (convection and friction), as well as the free convection with the external ambient, have a minor impact on the mean system response.

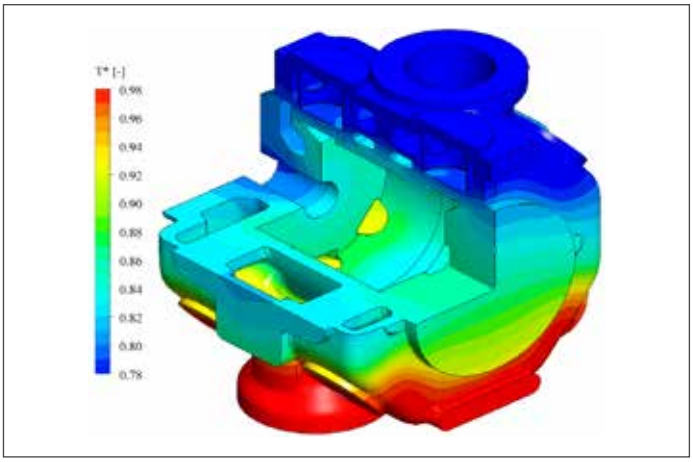

Figure 14 – Temperature field for the metal body (section view)

This latter observation justifies the use of a simplified approach for establishing the boundary conditions of both the external and compression chamber surfaces. Attention mainly should be focused on a reliable and accurate estimate of the gas ducts' HTC.

REGION	HEAT TRANSFER [%]
Cylinder Liner	6.6%
Cylinder Heads	6.3%
Suction Duct	-47.4%
Discharge Duct	141.4%
External Ambient	-6.9%

Table 5 – Contribution of the metal surfaces with respect to the overall heat absorbed by water

Conclusions

GE Oil & Gas performed a detailed investigation of a numerical methodology for the simulation of conjugate heat transfer of a water-cooled reciprocating compressor.

The CHT analysis aimed to accurately predict both the thermal state of the compressor cylinder and the temperature field of the cooling water.

Preliminary CFD simulations used to analyze the relevance of wall roughness and buoyancy on the thermal and fluid-dynamic conditions of the water showed that natural convection significantly prevailed in 88 percent of the fluid volume, while roughness had a negligible effect because most surfaces were in the hydraulically smooth regime.

Next, the assessment of appropriate thermal boundary conditions for the metal body in the water-metal coupled simulations was addressed. The results clearly showed that the largest amount of heat transfer is determined by forced convection inside the gas ducts. An accurate estimate of the *HTC* distribution is therefore necessary, and can be achieved through a specific CFD simulation.

In contrast, the use of simplified boundary conditions derived from literature correlations for both external surface and compression chamber was assumed to not significantly affect the accuracy of the results, due to the very small contribution to the overall heat transfer.

References

1 Possamai, F.C. and M.L. Todescat, 2004, "A review of household compressor energy performance," Int. Compressor Engineering Conference, Purdue University, Indiana.

2 Ooi, K.T., 2003, "Heat transfer study of a hermetic refrigeration compressor," Applied Thermal Engineering, 23(15), pp. 1931-1945.

3 Aigner, R. and Steinrück, H., 2007, "Modelling Fluid Dynamics, Heat Transfer and Valve Dynamics in a Reciprocating Compressor," Proc. of the 5th Conference of the EFRC, Prague, Czech Republic.

4 Disconzi, F.P., Deschamps, C.J. and Pereira, E.L.L., 2012, "Development of an In-Cylinder Heat Transfer Correlation for Reciprocating Compressors," Int. Compressor Engineering Conference, Purdue University, Indiana.

5 Abidin, Z., Almbauer, R., Burgstaller, A. and Nagy, D., 2006, "Domain Decomposition Method for 3-Dimensional Simulation of the Piston Cylinder Section of a Hermetic Reciprocating Compressor," Int. Compressor Engineering Conf., Purdue University, Indiana.

6 McAdams, W.H., 1954, Heat Transmission, 3rd Ed. McGraw-Hill, New York, NY.

7 Dittus, F.W. and Boelter, L.M.K., 1985, "Heat transfer in automobile radiators of the tubular type," Int. Comm. in Heat and Mass Transfer, 12(1), pp. 3-22.

8 Petukhov, B.S., 1970, "Heat Transfer and Friction in Turbulent Pipe Flow with Variable Physical Properties," Advances in Heat Transfer, 6, pp. 503-564.

9 Sleicher, C.A. and Rouse, M.W., 1975, "A convenient correlation for heat transfer to constant and variable property fluids in turbulent pipe flow," Int. Journal of Heat and Mass Transfer, 18(5), pp. 677-683.

10 Bhatti, M.S. and Shah, R.K., 1987, "Turbulent and transition convective heat transfer in ducts," Hand Book of Single Phase Convective Heat Transfer, Wiley, pp. 4.1–4.166.

11 Fagotti, F., Todescat, M.L., Ferreira, R.T.S. and Prata, A.T., 1994, "Heat transfer modeling in a reciprocating compressor," Int. Compressor Engineering Conference, Purdue University, Indiana.

12 Annand, W.J.D., 1963, "Heat Transfer in the Cylinders of Reciprocating Internal Combustion Engines," Proc. J. Mech. Engrs., 117(36), pp. 973-996.

13 Webb, R.L., Eckert, E.R.G., and Goldstein, R.J., 1971, "Heat Transfer and Friction in Tubes With Repeated-Rib Roughness," Int. J. Heat Mass Transfer, 14, pp. 601–617.

14 Ansys, Inc., ANSYS-CFX Solver Theory Guide, release 14.0.

15 Burck, E., 1969, "Influence of Prandtl Number on Heat Transfer and Pressure Drop of Artificially Roughened Channels," Heat and Mass Transfer, 2(2), pp. 87-98.

16 Adams, T., Grant, C. and Watson, H., 2012, "A Simple Algorithm to Relate Measured Surface Roughness to Equivalent Sand-grain Roughness," Int. J. of Mechanical Engineering and Mechatronics (ICMEM), 1(1), pp. 66-71.

17 Symolon, P., Neuhaus, W., Odell, R., 2005, "Mixed Convection Heat Transfer Experiments in Smooth and Rough Vertical Tubes," Transactions - American Nuclear Society, 92, pp. 387-390.

18 Wilcox, D.C., 1998, Turbulence Modeling for CFD, DCW Industries Inc, California.

19 Balduzzi, F., Ferrara, G., Maleci, R., Babbini, A. and Pratelli, G., 2014, "A Parametric CFD Analysis of the Valve Pocket Losses in Reciprocating Compressors," Paper accepted for publication in Journal of Pressure Vessel Technology.

20 Balduzzi, F., Ferrara, G., Babbini, A. and Pratelli, G., 2012, "CFD evaluation of the pressure losses in a reciprocating compressor: a flexible approach," Proc. of the ASME 11th ESDA Conference, Nantes, France.

21 Pratelli, G., Babbini, A., Balduzzi, F., Ferrara, G., Maleci, R., and Romani, L., 2012, "CFD Evaluation of Pressure Losses on Reciprocating Compressor Components," Proc. of the 8th Conference of the EFRC, Dusseldorf, Germany.

22 Schumann, U., 1988, "Minimum friction velocity and heat transfer in the rough surface layer of convective boundary layer," Boundary-Layer Meteorology, 44(4), pp. 311-326.

Imagination at work

GE Oil & Gas - Global Headquarters
The Ark - 201 Talgarth Road, Hammersmith - London, W6 8BJ, UK
T +44 207 302 6000
customer.service.center@ge.com

Nuovo Pignone S.p.A. - Nuovo Pignone S.r.l
Via Felice Matteucci, 2 - 50127 Florence, Italy
T +39 055 423 211
F +39 055 423 2800

Downstream Technology Solutions
4424 West Sam Houston Parkway North - Houston, TX 77041-8200, US

Reciprocating compressor cylinder's cooling: a numerical approach using computational fluid dynamics with conjugate heat transfer
By Francesco Balduzzi, Giovanni Ferrara, Alberto Babbini, Riccardo Maleci

GEA31969 (09/2015)